doi:10.1016/j.jmb.2004.11.025 J. Mol. Biol. (2005) 345, 1253–1264

JMB

Available online at www.sciencedirect.com

SCIENCE DIRECT®

ELSEVIER

The Structure of the *Arabidopsis thaliana* SOS3: Molecular Mechanism of Sensing Calcium for Salt Stress Response

María José Sánchez-Barrena[1], Martín Martínez-Ripoll[1], Jian-Kang Zhu[2] and Armando Albert[1]*

[1]*Grupo de Cristalografía Macromolecular y Biología Estructural, Instituto de Química Física "Rocasolano" Consejo Superior de Investigaciones Científicas Serrano 119, E-28006 Madrid Spain*

[2]*Department of Botany and Plant Sciences, and the Institute for Integrative Genome Biology 2150 Batchelor Hall, University of California, Riverside, CA 92521, USA*

**Corresponding author*

The *Arabidopsis thaliana* SOS3 gene encodes a calcium sensor that is required for plant salt tolerance. The SOS3 protein binds to and activates the self-inhibited SOS2 protein kinase, which mediates the expression and activities of various transporters important for ion homeostasis under salt stress. SOS3 belongs to a unique family of calcium-binding proteins that contain two pairs of EF hand motifs with four putative metal-binding sites. We report the crystal structure of a dimeric SOS3 protein in complex with calcium, and with calcium and manganese. Analytical ultracentrifugation experiments and circular dichroism measurements show that calcium binding is responsible for the dimerization of SOS3. This leads to a change in the global shape and surface properties of the protein that may be sufficient to transmit the Ca^{2+} signal elicited during salt stress.

Keywords: calcium signaling; protein structure; salt tolerance; crystallography; EF-hand

Introduction

Due to their sessile nature, plants have to endure adverse environmental conditions such as drought and soil salinity. Excess salts in the soil inhibit plant growth and cause great losses in agricultural productivity worldwide.[1,2] The excessive sodium ion (Na^+) present in saline soils is particularly harmful to plants because it is toxic to cellular enzymes if it accumulates to a high level in the cytoplasm. Therefore, maintaining a low concentration of Na^+ in the cytoplasm is key to plant salt tolerance.[1–3]

Genetic and biochemical studies in Arabidopsis have identified the salt overly sensitive (SOS) pathway for Na^+ homeostasis and salt tolerance.[3,4] In this pathway, SOS3 is a calcium-binding protein capable of sensing the cytosolic calcium ion (Ca^{2+}) signal elicited by salt stress.[5,6] SOS3 interacts physically with SOS2, a serine/threonine protein kinase.[7,8] In the presence of Ca^{2+}, SOS3 activates the substrate phosphorylation activity of SOS2. The binding of SOS3 to SOS2 is mediated by the 21 amino acid residue FISL motif in SOS2, which is autoinhibitory to the kinase activity.[9] SOS3 is myristoylated at its N terminus, and the myristoylation is important for recruiting SOS2 to the plasma membrane and for salt tolerance in plants.[6,10] Both SOS3 and SOS2 are required for the salt stress activation of SOS1, a Na^+/H^+ antiporter on the plasma membrane.[10,11] The SOS3–SOS2 kinase complex has been shown to phosphorylate SOS1.[10] Loss-of-function mutations in any of the SOS genes disrupts cellular sodium and potasium homeostasis, and render Arabidopsis plants hypersensitive to inhibition by salt stress.[4]

SOS3 is the founding member of a unique family of ten EF-hand type calcium-binding proteins in Arabidopsis. This family of proteins shares significant sequence similarities to the B subunit of calcineurin (i.e. phosphatase type 2B) and animal neuronal calcium sensors.[5,9] However, Arabidopsis clearly does not have any 2B-type protein phosphatase. Instead, members of the SOS3 family, known as SCaBPs[9] or CBLs,[12] interact with specific members of the SOS2-like family of protein kinases (PKS or CIPK[12]) to form distinct protein kinase complexes.[9,13] In plants, diverse environmental stimuli such as salinity, drought, cold, gravity, light, anoxia and mechanical perturbation all are

Abbreviations used: SOS, salt overly sensitive.

E-mail address of the corresponding author: xalbert@iqfr.csic.es

capable of eliciting Ca^{2+} signals.[14,15] The SCaBPs together with other EF-hand type calcium-binding proteins may be able to distinguish different Ca^{2+} signals, and transduce the signals to regulate various effector proteins, generating appropriate cellular responses.[13,14]

In order to understand how SOS3 senses Ca^{2+} and regulates SOS2, and ultimately how it functions specifically to mediate signaling by salt stress but not other stresses that also cause changes in the cytosolic free Ca^{2+}, it is important to solve the three-dimensional structure of SOS3. Here, we report the crystal structure of an SOS3 dimer in complex with Ca^{2+}, and with Ca^{2+} and manganese ion (Mn^{2+}), at 2.75 Å and at 3.0 Å resolution, respectively. The structure suggests a mechanism for Ca^{2+}-sensing by SOS3 and for the activation of its interacting partner, SOS2.

Results and Discussion

SOS3 displays a calmodulin-like fold

The X-ray structure of SOS3 in complex with Ca^{2+}, and with Ca^{2+} and Mn^{2+} was solved by single anomalous scattering phasing provided by seven iodine atoms at 2.75 Å and 3.00 Å, resolution respectively (Figure 1; and see Materials and Methods). The structures of both complexes were refined independently to avoid refinement bias. However, these structures are nearly identical (C^{α} backbone root-mean-square deviation, RMSD of 0.2 Å);[16] hence, unless stated otherwise, all the results presented here are referred to the SOS3 Ca^{2+} complex.

The overall fold of an SOS3 protomer is almost identical with that found for SCaBP1/AtCBL2[17] and the homologous structures of calcineurin B (CnB)[18] and neuronal calcium-sensor (NCS1).[19] To summarize, SOS3 can be described as a two-domain structure connected by a short linker. Each domain is formed by a pair of adjacent EF-hand motifs. The N-terminal domain contains an additional α-helix and the C-terminal domain a small α-helix plus an unstructured tail that protrudes towards the N-terminal domain.

The dimeric structure of SOS3

Sedimentation equilibrium experiments were performed to investigate the association state of SOS3 in solution and the effect of Ca^{2+} and other physiologically relevant metal ions on SOS3 oligomerization (Table 1; and see Materials and Methods). Our data show that SOS3 displays a monomer/dimer equilibrium with a dimerization constant of around $5\times10^{4}\,M^{-1}$. However, the analysis of the auto-association equilibrium of SOS3 as a function of the concentration of Ca^{2+} shows that the fraction of dimer increases with the concentration of free Ca^{2+} (Table 1). We do not observe any effect of Mn^{2+} or Mg^{2+} on the oligomeric state of SOS3 in solution (data not shown).

The analysis of the crystal structure of SOS3 reveals that the protein is a dimer as observed in solution with a 2-fold symmetry axis coincident with the crystallographic 2-fold axis (Figure 1). Hence, only a peptidic subunit is found in the asymmetric unit. The crystallographic dimer displays a V shape. Molecules within the dimer interact through the C-terminal end of helix F3, the N-terminal end of helix E4 and the loop connecting both helices. There is a 4% decrease in the solvent-accessible surface area per protomer in the formation of the dimer; and 80% of this occluded area corresponds to hydrophobic residues.[20] The dimerization involves the formation of one hydrogen bond between Ser144 OG and its symmetry-related residue. These values are lower than those expected for stable homodimers in solution, but are similar to those corresponding to other signal transduction complexes.[21–23] These complexes and SOS3 show a transient oligomerization state that is dependent on factors such as an increase in the local concentration of the protein, the binding of a particular ligand or a change in the local physicochemical environment. SOS3 dimer displays a structure that exposes to the solvent eight metal-binding sites, the N-terminal myristoylation sites, and the C-terminal end of the protein, which has been shown to be essential for SOS2 interaction and subsequent activation.[6]

Ishitani *et al*. showed that SOS3 myristoylation is necessary for SOS2 activation but may not be for membrane association in plant cells.[6] SOS3 presents a sequence of five lysine residues at the N-terminal end, which may be sufficient for membrane anchorage.[24,25] This suggests that myristoylation adds a structural determinant for the correct positioning of SOS3 with respect to the membrane. Dimeric SOS3 duplicates the efficiency of the membrane binding with respect to the monomer and would help in positioning the macromolecule, as it provides two accessible anchoring points.

The metal-binding sites of SOS3

The classical EF-hand motif is characterized by a sequence of 12 residues involved in Ca^{2+} binding (Figure 2). The amino acid residues in positions X, Y, Z and −Z ligate Ca^{2+} *via* side-chain oxygen donors. The residues at −X and −Y participate in the coordination of the metal with a backbone oxygen atom and with a water-mediated interaction, respectively. Sequences of the EF motifs in SCaBPs are different from the classical sequences, since the oxygen donor at position Y is replaced by a hydrophobic or basic amino acid residue for EF1 and for EF2, EF3 and EF4, respectively. In addition, the EF1 motif contains an insertion of two amino acid residues between the X and Y positions.[9,26]

Both the experimental and the omit electron density maps at SOS3 metal-binding sites allowed

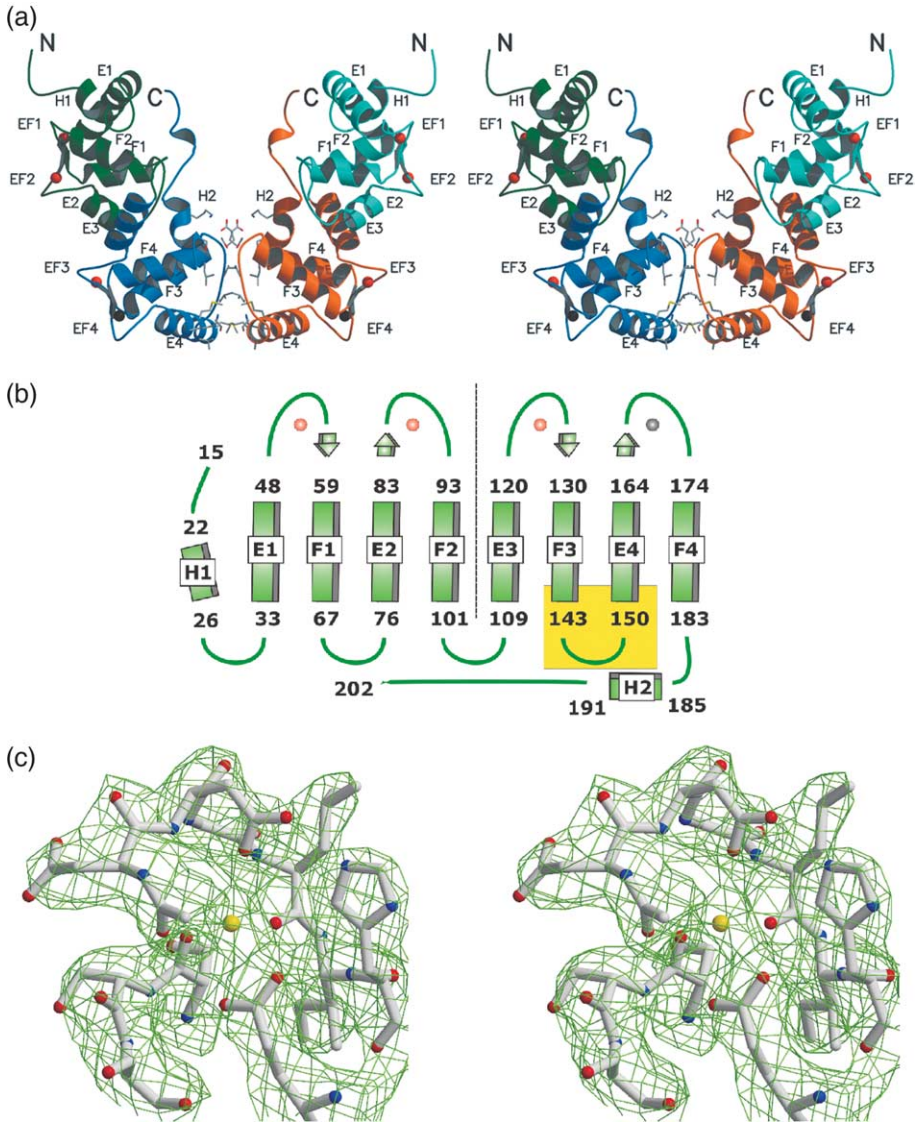

Figure 1. (a) Stereoview of the ribbon structure representation of SOS3 showing the domain structure of the protein. Amino acid side-chains involved in the formation of the dimer are displayed in stick mode. Calcium and manganese ions are displayed as red balls and black balls, respectively. (b) A representation of the topology of SOS3. Secondary structural elements are defined by RasMol.[56] Elements involved in dimerization are highlighted with a yellow rectangle. A broken line separates the N-terminal domain and the C-terminal domain. The amino acid residues not defined in the crystal structure are displayed in the one-letter code. (c) A section of the experimental electron density map (contoured at 1σ) at the Ca^{2+}-binding site EF1 of SOS3.

an unambiguous positioning of four Ca^{2+} and all their peptidic ligands (Figure 1(c)). The joined analysis of the structure of metal-binding sites of SOS3 and SCaBP1/AtCBL2 reveals a unique binding mode for the SCaBP/CBL family of proteins. The SCaBPs Ca^{2+}-binding sites substitute the side-chain oxygen donor at position Y by a backbone carbonyl group and the EF1 loop rearranges to accommodate the insertion of two residues (Figure 2). Interestingly, despite these differences, no significant change is observed in the coordination geometry of Ca^{2+} when the structures of

Table 1. Oligomeric state of SOS3 in solution as a function of protein and Ca^{2+} concentrations

[SOS3]:[Ca^{2+}]	1 : 0	0.5 : 0	1 : 1	1 : 3	1 : 10	1 : 30	1 : 100
Molecular mass (kDa)	42.1	37.1	42.1	44.4	45.7	47.5	50.6
Fraction of dimer, α	0.45	0.27	0.45	0.55	0.61	0.71	0.90

[SOS3]:[Ca^{2+}] stands for the ratio between the concentrations of SOS3 and Ca^{2+}. Data are referred to [SOS3]$=2.72\times10^{-5}$ M. The calculated molecular mass of SOS3 is 26.0 kDa.

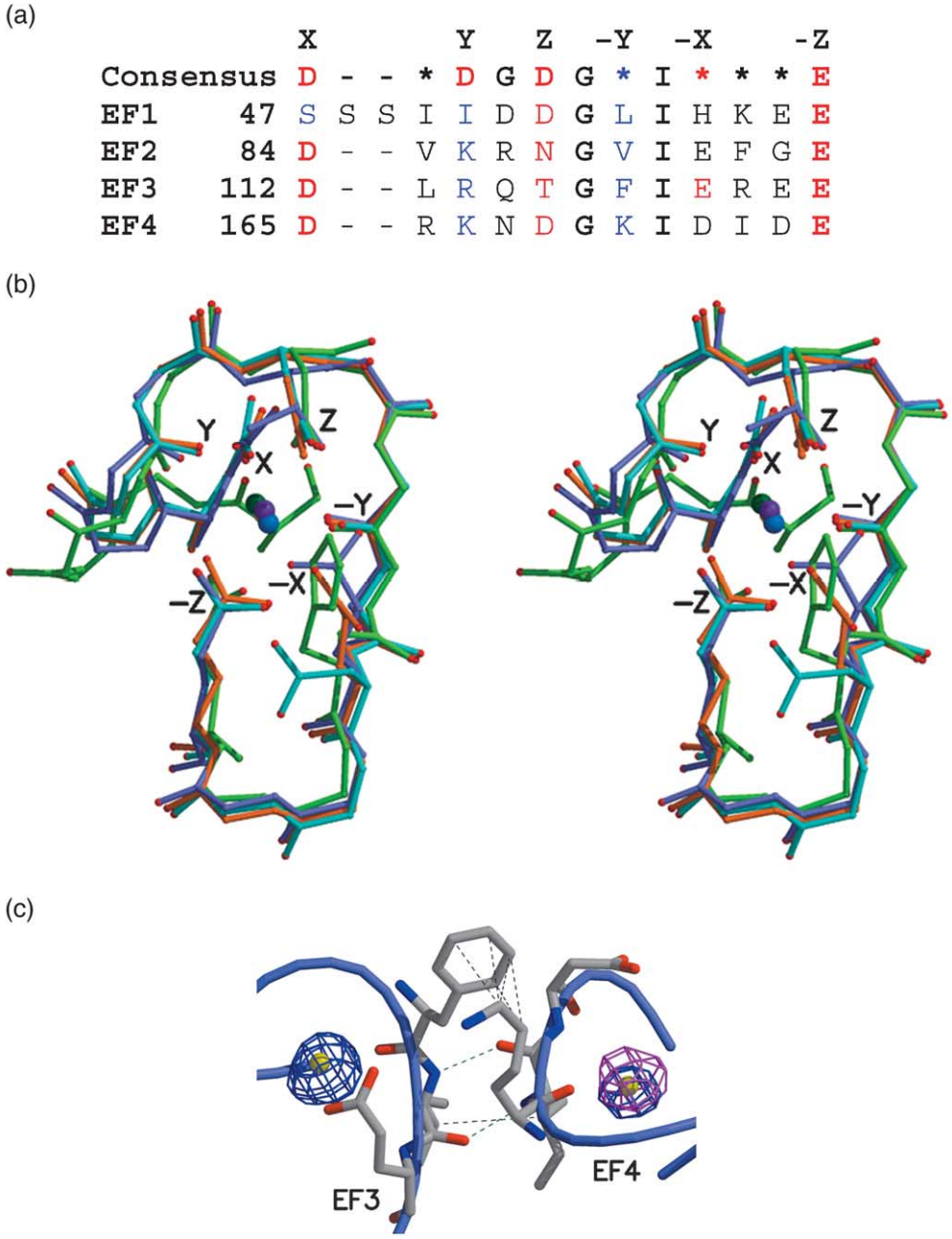

Figure 2. (a) A comparison of the sequence of the EF Ca^{2+}-binding sites of SOS3 and the classical EF-hand superfamily. Residues involved in Ca^{2+} binding are highlighted by X, Y, Z, −X, −Y, −Z according to a classical EF hand. Red and blue colors stand for side-chain or main-chain oxygen donor, respectively. (b) Stereoview of the structural superposition of Ca^{2+}-binding sites of SOS3. EF1, EF2, EF3 and EF4 are depicted in green, cyan, orange and lilac, respectively. Oxygen atoms are displayed in red. (c) The interactions between EF3 and EF4 sites of SOS3. Green and black broken lines stand for hydrogen bonds and for hydrophobic interactions, respectively. Ca^{2+} sites are depicted as yellow balls. Two sections of the electron density omit map (contoured at 4σ) of SOS3 Ca^{2+} complex and the anomalous difference electron density map (contoured at 4σ) of SOS3 Ca^{2+} Mn^{2+} complex are depicted in blue and magenta, respectively.

SCaBPs and a classical EF-hand are compared. Ca^{2+} coordinates seven protein oxygen atoms at site EF3 and six protein oxygen atoms and a water molecule at site EF4. In both cases the metal ion displays the classical bipyramidal pentagonal coordination geometry. On the other hand, Ca^{2+} at sites EF1 and EF2 coordinates only six oxygen ligands, since the interaction between side-chains at positions Z and −X hinders the approach of another ligand.

Both the N-terminal domain and the C-terminal domain display a short antiparallel β sheet located between adjacent metal-binding sites. These β sheets are stabilized by the hydrophobic interaction

between the side-chains of the residues at position −Y and the conserved isoleucine residue at position −Y+1 (Figures 1 and 2). These interactions suggest that SOS3 displays cooperativity in the Ca^{2+} binding between adjacent EF hands, as has been observed for other proteins of the EF hand superfamily.[27–30] For calmodulins, cooperativity ensures that a full activation occurs in a narrow region of Ca^{2+} concentration during a signaling event. Remarkably, this pattern of interactions is not conserved in the structure of SCaBP1/AtCBL2, where the cooperativity is not observed, since it displays only one functional EF hand in each domain. This may be sufficient for a differential transduction of the Ca^{2+} signal by SOS3 and by SCaBP1/AtCBL2.

The crystal structures of SOS3 in complex with Ca^{2+} and with Ca^{2+} and Mn^{2+} are identical, with changes confined to the EF4 metal-binding site. The anomalous difference map calculated with diffraction data collected at a wavelength of 1.75 Å was used to demonstrate the presence of Mn^{2+} solely at site EF4 (Figure 2(c)). Our data show that Mn^{2+} displays the same coordination as that observed for Ca^{2+}.

The thermal denaturation of a protein at increasing concentrations of a ligand can be used to test if a protein binds a particular ligand.[31] Consequently, we monitored the thermal stability of SOS3 in the presence of increasing concentrations of different metal ions by circular dichroism spectroscopy (Materials and Methods, and see Figure 3). Native protein purified as described in Materials and Methods was used as a control. Our results show that only Ca^{2+} and Mn^{2+} are able to bind SOS3, since they induce a change in the thermal denaturation temperature (T_m) of the protein. The presence of an excess of EDTA in the medium precludes any variation of the T_m. The analysis of the variation of T_m with the concentration of the ligand indicates that the apparent averaged affinity of SOS3 for Mn^{2+} is at least one order of magnitude higher than that observed for Ca^{2+}. This is not surprising, since the concentration of Ca^{2+} in the cytosol should be much higher than that expected for Mn^{+2}. Mn^{2+} binding to SOS3 may be biologically relevant, since SOS2 kinase and other protein kinases from the PKS/CIPK family display enhanced activity when Mn^{2+} acts as a cofactor.[12,32,33] Hence, SOS3 or other SCaBP/CBL proteins could act as a carrier for this cofactor or, alternatively, could buffer the availability of free Mn^{2+} to prevent a constitutive activation of the kinase. However, to address this question, it would be necessary to characterize the affinity of this group of proteins for Mn^{2+} and to measure the concentration of free Mn^{2+} in the cytosol.

As mentioned above, Ca^{2+} triggers the dimerization of SOS3. It is likely that the binding at sites EF3 and EF4 is responsible for the self-association of the macromolecule, since they are closer than EF1 and EF2 to the dimerization interface (Figure 1(a)). However, the sedimentation equilibrium experiments show that Mn^{2+} does not affect the dimerization equilibrium of SOS3. This suggests that Ca^{2+} binding at site EF3 stabilizes the dimer in solution, as Mn^{2+} binds only to EF4. The fact that a deletion of three amino acids at EF3 produces a non-functional mutant protein[6] suggests that Ca^{2+} binding at EF3 and probably dimerization are physiologically relevant.

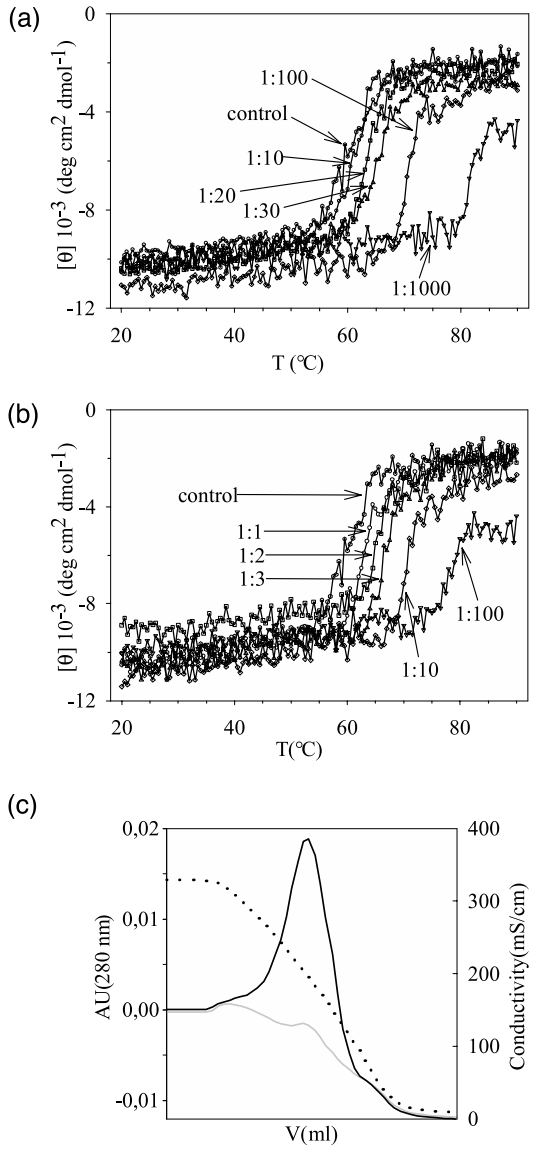

Figure 3. Comparison of the circular dichroism denaturation profiles of SOS3 as a function of (a) Ca^{2+} and (b) Mn^{2+} concentrations. The SOS3:metal ion ratio ([SOS3]:[Ca^{2+}]) stands for the relationship between the molar concentrations of protein and metal ion in the solution. Data are referred to [SOS3] = 7.7×10^{-6} M. Profiles corresponding to [SOS3]:[Ca^{2+}] ratio 1 : 3 and 1 : 6 are omitted for clarity. [θ] stands for the mean residues ellipticity. (c) Hydrophobic interaction chromatography of SOS3. The dotted line represents the conductivity of the solution. The black and grey lines represent the absorbance recorded at 280 nm in the absence or in the presence of 10 mM $CaCl_2$, respectively.

SOS3 enhances its hydrophobic character upon calcium binding

As mentioned in Introduction, the SOS2 family of protein kinases interacts with the SCaBPs through a hydrophobic conserved motif of 21 amino acid residues known as the FISL motif.[9] Hence, it would be expected that calcium activation of SOS3 and subsequent dimerization would enhance the hydrophobic character of the molecular surface of the macromolecule. In order to assess this hypothesis, we performed a hydrophobic interaction chromatography with SOS3. This method is based on the varying strengths of the hydrophobic interactions of proteins with hydrophobic ligands immobilized to a matrix. A moderately high concentration of salt promotes adsorption of the biomolecules and a linear decrease in salt concentration leads to the elution according to their increased hydrophobicity. In a Ca^{2+}-free medium, SOS3 elutes at a medium concentration of salt. On the other hand, in the presence of Ca^{2+}, SOS3 is adsorbed strongly to the resin even at low concentrations of salt. The elution is achieved by adding EDTA to the column. (Figure 3(c); and see Materials and Methods).This demonstrates that Ca^{2+} induces a conformational change in SOS3 leading to an increased exposure of hydrophobic residues.

The structural comparison of SOS3 and SCaBP1/AtCBL2 suggests a model for sensing Ca^{2+}

The main differences between SOS3 and the structural homologs arise from the relative positions of the N and C-terminal domains. This can be measured as the rotation angle that relates the C-terminal domains and the distance between the corresponding centers of mass when the N-terminal domains of the structural homologs are superimposed on that of SOS3. Table 2 shows these parameters together with the sequence identity and the RMSD of the C^{α} backbone of SOS3 with respect to SCaBP1/AtCBL2, CnB and NCS1. These data indicate that there is no relationship between the differences between domains, the local RMSD and the sequence identity. Rather, as discussed by Nagae *et al.*,[17] local changes motivated by sequence differences at loop regions should account for the structural changes among the proteins of the family. However, SOS3 and SCaBP1/AtCBL2 display the largest differences in the relative position of the N terminus and the C terminus, despite the fact that they share the highest level of sequence identity, have no insertion at loops and belong to the same family of proteins. This suggests that local differences motivated by Ca^{2+} binding could be responsible for global changes in the structure, as has been reported for other EF hand proteins.[26,34] SCaBP1/AtCBL2 binds Ca^{2+} at sites EF1 and EF4, whereas EF2 and EF3 display an open conformation stabilized by electrostatic interactions and a water molecule. The structural comparison of SOS3 and SCaBP1/AtCBL2 at these sites reveals noticeable differences between the relative positions of helices E2 and F2, and E3 and F3. Figure 4 shows the superposition of the EF2 and EF3 sites from SOS3 and SCaBP1/AtCBL2. As can be seen, the interaction of a glutamate side-chain at position $-Z$ with Ca^{2+} motivates a general displacement of helix F2 or F3 with respect to helix E2 or E3. These rearrangements upon Ca^{2+} binding could be responsible for the large change in the relative positions of the N and C-terminal domains, since EF2 and EF3 are in the interdomain interface.

The structural differences between SOS3 and SCaBP1/AtCBL2 reflect a change in the global shape and properties of the macromolecule surface that facilitates dimer formation. As mentioned above, SOS3 displays a large accessible hydrophobic path at the dimerization interface, which is around 25% larger than the hydrophobic accessible area observed in SCaBP1/AtCBL2 in this region.[20] In addition, the relative position of the N-terminal domain with respect to the C-terminal domain of SCaBP1/AtCBL2 would hinder the formation of the dimer. This fact suggests that calcium binding, domain swiveling and dimerization are coupled processes in SOS3. Unfortunately, there are no biophysical data on the oligomerization state of other SCaBP/CBL proteins; however, the high level of sequence homology shared by the family of proteins suggests that other members of the SCaBP/CBL would display the same mechanism of calcium regulation based on the dimerization.

Nagae *et al.*[17] suggest that the recognition mechanism between SCaBP1/AtCBL2 and its kinase target is similar to that observed for CnB and calcinerurin A (CnA). CnA expands a helix to a

Table 2. Comparison between SOS3 and SCaBP1/AtCBL2, CnB and NCS1

		SCaBP1	CnB	NCS1
SOS3	Identity (%)	50.4	19.8	26.6
	Domain swiveling (deg.)	33	26	24
	Distance between C_M (Å)	4.3	3.2	1.4
	RMSD for the N-term domain (Å)	1.73 (77)	1.05 (70)	1.41 (74)
	RMSD for the C-term domain (Å)	1.22 (84)	1.38 (69)	1.63 (67)

Values within parentheses stand for the number of equivalent (cut-off distance of 3.5 Å) C^{α} atoms in the structural alignment. C_M stands for the center of mass. The PDB codes are 1UHN, 1AUI and 1G8I for SCaBP1/AtCBL2, CnB and NCS1, respectively.

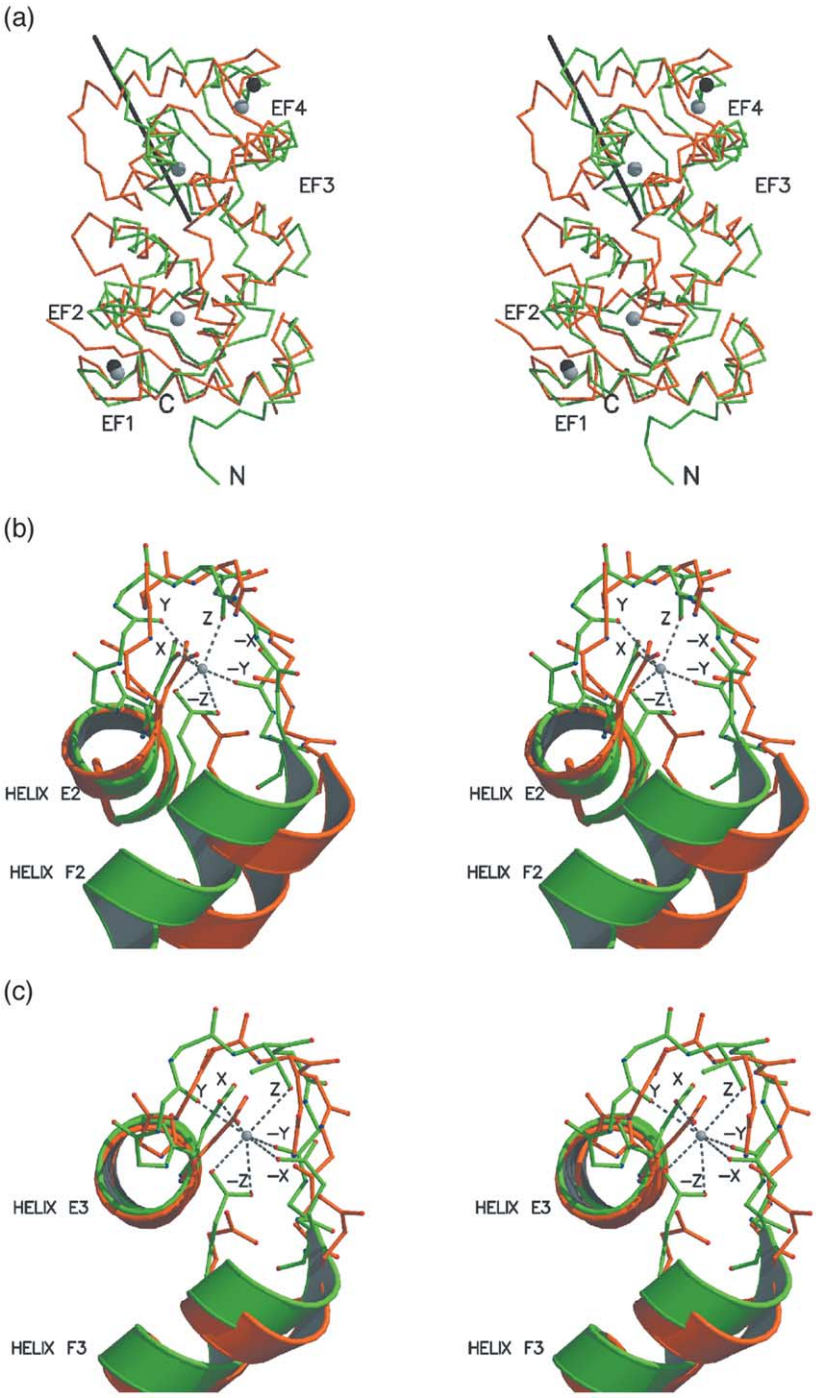

Figure 4. Stereoviews comparing the X-ray structures of SOS3 (green) and AtCBL2 (orange). (a) Backbone differences when the N-terminal domains are superimposed. Ca^{2+}-binding sites are displayed as gray and black balls for SOS3 and AtCBL2, respectively. The black stick represents the rotation axis relating the C-terminal domains. (b) and (c) Structural differences at EF2 and EF3 sites when helices E2 and E3, respectively, are superimposed.

hydrophobic crevice defined between the C-terminal tail and the loops F2-E3 and F3-E4 of CnB. The monomeric SCaBP1/AtCBL2 displays a close conformation of the crevice and it is suggested that Ca^{2+} would induce a domain swiveling, leading to a molecular conformation that would expose the hidden hydrophobic residues of this cavity. This would allow the interaction of SCaBP1/AtCBL2 with the FISL motif of the corresponding kinase. However, the structural analysis of SOS3 suggests that the activation of SOS2 could follow a different mechanism. The structural superposition of the fully Ca^{2+}-occupied SOS3 and SCaBP1/AtCBL2 shows that the swiveling between domains tends to close the crevice. In addition, the dimeric structure of SOS3 would preclude the interaction between SOS3 and SOS2 in the manner observed in the CnA–CnB complex. Rather, the analysis of the molecular surface properties of SOS3 indicates that there are two hydrophobic patches that are located at the interdomain and the intersubunit interfaces. In addition, the electron density at the F2-E3 loop suggests some degree of mobility for this region of the protein. This loop is highly charged, since it displays sequence Arg-Asn-Arg-Asn-Arg-Arg-Asn and it is shielding a group of hydrophobic residues.

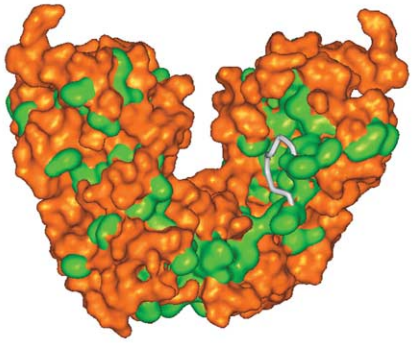

Figure 5. Molecular surface representation of SOS3. SOS3 is rotated 15° along the dimer axis from the view shown in Figure 1. Hydrophobic residues are depicted in green. The mobile loop from A67 to A73 has been excluded from the surface calculation and is represented as a white ribbon.

These occluded residues, together with other hydrophobic residues at the molecular surface of the dimeric SOS3, form an elongated patch involving both subunits within the dimer that may interact with the hydrophobic FISL motif from SOS2 (Figure 5).

Conclusions

The crystal structure of Ca^{2+}-bound dimeric SOS3, together with the biophysical characterization of the macromolecule in solution, suggest a mechanism for molecular function of SOS3 and for the activation of its molecular partner, the kinase SOS2. Our data show that SOS3 is able to sense the cytosolic Ca^{2+} signal elicited by salt stress.[3] We show that this promotes the dimerization of the macromolecule and a conformational change that reflects an increase of the hydrophobic character of the macromolecule. These changes would be sufficient to transmit the Ca^{2+} signal to SOS2, since they involve a dramatic modification of the global shape and molecular surface properties of the macromolecule.

Materials and Methods

Protein preparation, crystallization and data collection

SOS3 was obtained from cultures of *Escherichia coli* and purified to homogeneity as described by Sánchez-Barrena *et al*.[35] To summarize, the overexpressed His-tagged protein was purified in two steps. First, a protocol for nickel-affinity chromatography followed by an in-column cleavage with thrombin protease (Amersham Biosciences Limited, UK) was developed. Second, SOS3 was loaded onto a Resource-Q anionic-exchange column (Amersham Biosciences Limited, UK) and eluted with a NaCl gradient from 50 mM to 0.5 M. Pure protein was treated with a chelating resin (Hampton Research, CA, USA) that complexes preferentially divalent metal ions.[36] Finally, the protein was concentrated to 15 mg/ml in 20 mM Tris–HCl (pH 7.5), 50 mM NaCl.

Prior to crystallization, the protein was incubated with 3.8 mM $CaCl_2$ (SOS3-Ca) and with 3.8 mM $CaCl_2$ plus 3.8 mM $MnCl_2$ (SOS3-Ca-Mn) to reach a final protein concentration of 10 mg/ml and a protein to metal molar concentration ratio of 1 : 10 and 1 : 10 : 10, respectively. Crystallization experiments were carried out at room temperature. Crystals corresponding to the SOS3 Ca^{2+} complex were grown using vapor-diffusion techniques from drops containing SOS3-Ca, reservoir solutions (24% (w/v) methyl-pentanediol (MPD), 18% (w/v) polyethylene glycol 4000 and 0.1 M sodium citrate, pH 4.8) and 1 M NaI in a ratio of 2 : 1 : 0.75 (by vol.). Crystals corresponding to the SOS3 Ca^{2+} Mn^{2+} complex were also grown with the same crystallization technique and solutions except that the concentration of polyethylene glycol 4000 in the reservoir solution was 16% (w/v).

Crystals were mounted in a fiber loop and frozen at 100 K in a nitrogen stream. No cryoprotectant solution was employed, since the reservoir solution had cryoprotectant properties.

X-ray diffraction data were collected in a CCD detector using the ESRF Grenoble synchrotron radiation source at wavelengths 0.92 Å and 1.75 Å at the BM16 beam-line. Diffraction data were processed using MOSFLM (Table 3).[37]

Structure determination

Attempts to solve the X-ray structure of SOS3 by molecular replacement using the coordinates of the homologous structure AtCBL2/SCaBP1 failed (AMoRe,[38] MOLREP[39]). However, a poor solution was found using the structure of the neuronal calcium-sensor 1 (NCS1) (PDB code 1G8I) as a search model.[40] Using this solution, it was possible to identify seven iodine atoms in the asymmetric unit (a.u.). Then, the structure of SOS3 was solved by single anomalous scattering (SAD), using the anomalous information corresponding to the iodine atoms from diffraction data of the SOS3 Ca^{2+} complex, collected at wavelength 1.7 Å.[41,42] Refinement of the iodine substructure and phasing were performed using SHARP.[43] Solvent-flattening was performed with DM[44] and SOLOMON,[45,46] using the SHARP protocols.

The solvent-flattened electron density map was good enough (Figure 1(c)) to trace an initial model that was first refined using the simulated annealing routine of CNS.[47] Several cycles of restrained refinement with REFMAC5[48] and iterative model building with O[49] were carried out. Water structure and two molecules of MPD from the solvent were also modeled. The myristoylation site (N terminus) and the C terminus of the protein appear disordered in the crystal and it was not possible to model these parts of the macromolecule. The refined structure of SOS3 in the presence of Ca^{2+} at 2.75 Å resolution (data measured at wavelength 0.92 Å) was used to solve the structure of the SOS3 Ca^{2+} Mn^{2+} complex (Table 3). The difference anomalous electron density map calculated from the diffraction data of the SOS3 Ca^{2+} Mn^{2+} complex corresponding to the wavelength 1.75 Å was used to identify a Mn^{2+} at EF4. Calculations were performed using CCP4 programs.[50]

The stereochemistry of the models was verified with PROCHECK.[51] Ribbon Figures were produced using

Table 3. Data collection, structure solution and refinement statistics

	SOS3 Ca^{2+} complex		SOS3 Ca^{2+} Mn^{2+} complex	
A. *Data collection*				
Wavelength (λ) (Å)	0.92	1.75	0.92	1.75
Space group	$I4_1$		$I4_1$	
Unit cell parameters				
a (Å)	91.6		91.9	
b (Å)	91.6		91.9	
c (Å)	85.4		85.6	
Resolution (Å)	62.0–2.75	45.6–2.8	46.0–3.0	49.9–3.0
$I/\sigma(I)$	4.5 (1.8)	2.6 (1.4)	4.5 (1.5)	2.6 (1.9)
R_{merge}[a] (%)	5.7 (41.8)	11.7 (47.5)	8.6 (51.2)	10.6 (39.7)
Completeness (%)	100 (100)	100 (100)	97.7 (97.7)	96.7 (96.7)
Multiplicity	3.7 (3.7)	7.5 (7.4)	4.5 (4.5)	3.9 (3.8)
Temperature (K)	100	100	100	100
B. *Structure solution*				
Number of sites		7		
R_{Cullis}[b]		0.68		
Phasing power[b]		1.65		
FOM[b]		0.30		
C. *Refinement*				
Resolution range (Å)	20–2.75		20–3.0	
R-factor (%)	23.5 (41.6)		23.7 (32.9)	
R_{free} (%)	26.4 (37.1)		26.2 (39.8)	
Number of atoms	1614		1614	
Number of reflections	9213		6609	
D. *Model*				
Molecules per a.u.	1		1	
Solvent content (%, v/v)	64.3		64.7	
Amino acid residues	188		188	
Calcium ions	4		3	
Manganese ions	0		1	
Iodine ions	7		7	
MPD molecules	2		2	
Water molecules	40		40	
RMS deviation:				
Bond lengths (Å)	0.014		0.016	
Bond angles (deg)	1.735		1.926	
Planar groups (A)	0.005		0.006	
Remarks	Residues A1–A14 and A203–A222 are not included in the model. The loop A67–A75 displays poor electron density.			

[a] $R_{merge} = \sum_{hkl} |I_{hkl} - \langle I_{hkl} \rangle| / \sum_{hkl} I_{hkl}$. Values in parentheses are for the highest-resolution shell: 2.90–2.75 Å and 2.95–2.80 Å (for processing statistics of the SOS3 Ca^{2+} complex and λ 0.92 Å and 1.75 Å, respectively), and 3.16–3.00 Å (for processing statistics of the SOS3 Ca^{2+} Mn^{2+} complex). The highest-resolution shell for refinement statistics are 2.82–2.75 Å (for the SOS3 Ca^{2+} complex) and from 3.08–3.00 Å (for the SOS3 Ca^{2+} Mn^{2+} complex).

[b] R_{Cullis}, Phasing power and FOM stand for the phasing statistics determined by SHARP.[42] Solvent content calculations were performed following Andersson & Hovmöller.[57]

MOLSCRIPT[52] and Raster3D.[53] The accessible surface area of SOS3 dimer and protomer was calculated with the program NACCESS from the LIGPLOT package.[20] The domain swiveling angles of SOS3, NCS1, AtCBL2/SCaBP1 and CnB were calculated with the program FIT†. Sequence alignment data were developed with BLAST.[54] The molecular surface of SOS3 dimer Figure was produced with Web Lab‡.

Sedimentation equilibrium

Sedimentation equilibrium experiments were performed in a Beckman Optima XL-A ultracentrifuge using a Ti50 rotor and six-channel centerpieces of Epon-charcoal (optical pathlength 12 mm). Samples of SOS3 were equilibrated against 20 mM Tris–HCl (pH 7.5), 50 mM NaCl buffer plus Ca^{2+}, Mn^{2+} and Mg^{2+} when appropriate (Table 1), and were centrifuged at 17,000 rpm, 20,000 rpm and 29,000 rpm and 20 °C. Radial scans at 280 nm were taken at 12 hours, 14 hours and 16 hours. The three scans were identical (equilibrium conditions were reached). The weight-average molecular mass (M_w) of SOS3 was determined by using the program EQASSOC with the partial specific volume of SOS3 set to 0.730 at 20 °C as calculated from its amino acid composition. Calculations were performed with data at 17,000 rpm. The dimerization constant (*K*) and the fraction of dimer in solution (α) were calculated from the observed M_w as a function of the concentration of protein and Ca^{2+}, following Rivas *et al*.[55]

Circular dichroism spectra

Circular dichroism spectra were recorded in a JASCO J-810 spectropolarimeter. Far-UV spectra were recorded

† http://bioinfo1.mbfys.lu.se/~guoguang/fit.html
‡ http://www.msi.com

in a 0.1 cm pathlength quartz cell, at a protein concentration of 0.2 mg/ml (7.7×10^{-6} M). Near-UV CD spectra were registered at protein concentration of 0.5 mg/ml (1.9×10^{-5} M) in a 1 cm pathlength quartz cell. The observed ellipticities were converted to mean residue ellipticities [θ] using an average molecular mass per residue of 115.4 Da. Thermal denaturation was monitored at a wavelength of 222 nm by increasing the temperature from 20 °C to 90 °C at 30 deg. C/hour and allowing the temperature to equilibrate for one minute before recording the spectra.

Samples were prepared as for sedimentation equilibrium experiments. Native protein obtained for purification was considered as a control. Far and near-UV spectra and the thermal denaturation profiles were recorded for: (i) the native protein; (ii) the native protein in the presence of Na^+, K^+, Rb^+, Cs^+, Ni^{2+}, Mg^{2+}, in SOS3:metal ion molar concentration ratios of 1 : 10 and 1 : 100 (data not shown); (iii) the native protein in the presence of Ca^{2+} in molar concentration ratios of 1 : 3, 1 : 6, 1 : 10, 1 : 20, 1 : 30, 1 : 60, 1 : 100 and 1 : 1000 (Figure 3(a)); (iv) the native protein in the presence of Mn^{2+} in molar concentration ratios 1 : 1, 1 : 2, 1 : 3, 1 : 10 and 1 : 100 (Figure 3(b)).

Hydrophobic interaction chromatography

Native SOS3 (0.22 mg) was loaded onto a phenyl Sepharose column (Amersham Biosciences Limited, UK) previously equilibrated with buffer 1 (1.7 M ammonium sulfate, 20 mM Tris–HCl (pH 7.0), 0.05% (w/v) NaN_3) and subjected to a washing step with five column volumes of buffer 1, followed by a gradient step of 20 column volumes with an ammonium sulfate gradient from 1.7 M to 0 M. In these conditions, SOS3 elutes at 0.9 M ammonium sulfate (Figure 3(c)). The same chromatographic steps were performed in the presence of 10 mM $CaCl_2$. In these conditions, SOS3 does not elute from the column. Elution was achieved by removal of bound calcium with 45 mM Tris–HCl (pH 7.0), 10 mM EDTA.

Protein Data Bank accession numbers

The coordinates and structure factors amplitudes of SOS3 Ca^{2+} and SOS3 Ca^{2+} and Mn^{2+} complexes have been deposited in the PDB with accession codes 1V1G and 1V1F, respectively.

Acknowledgements

We thank Dr M. Menéndez for critical comments on the manuscript and Dr J. L. Saiz-Velasco for the analytical ultracentrifugation data analysis. M.J.S.-B. was supported by an F.P.U. studentship from Ministerio de Educación, Cultura y Deporte. A.A. thanks the ESRF (Spanish beam-line BM16) for the access to the synchrotron radiation source. This work was funded by BMC2002-04011-C05-03 grant of the Spanish "Plan Nacional" (MCYT) to A.A. and by US National Institutes of Health grant R01GM59138 to J.K.Z.

References

1. Tester, M. & Davenport, R. (2003). Na^+ tolerance and Na^+ transport in higher plants. *Ann. Bot. (London)*, **91**, 503–527.
2. Hasegawa, P. M., Bressan, R. A., Zhu, J. K. & Bohnert, H. J. (2000). Plant cellular and molecular responses to high salinity. *Annu. Rev. Plant Mol. Plant Physiol.* **51**, 463–499.
3. Zhu, J. K. (2003). Regulation of ion homeostasis under salt stress. *Curr. Opin. Plant Biol.* **6**, 441–445.
4. Zhu, J. (2000). Genetic analysis of plant salt tolerance using *Arabidopsis thaliana*. *Plant Physiol.* **124**, 941–948.
5. Liu, J. & Zhu, J. K. (1998). A calcium sensor homolog required for plant salt tolerance. *Science*, **280**, 1943–1945.
6. Ishitani, M., Liu, J., Halfter, U., Kim, C. S., Shi, W. & Zhu, J. K. (2000). SOS3 function in plant salt tolerance requires N-myristoylation and calcium binding. *Plant Cell*, **12**, 1667–1678.
7. Liu, J., Ishitani, M., Halfter, U., Kim, C. S. & Zhu, J. K. (2000). The *Arabidopsis thaliana SOS2* gene encodes a protein kinase that is required for salt tolerance. *Proc. Natl Acad. Sci. USA*, **97**, 3730–3734.
8. Halfter, U., Ishitani, M. & Zhu, J. K. (2000). The *Arabidopsis* SOS2 protein kinase physically interacts with and is activated by the calcium-binding protein SOS3. *Proc. Natl Acad. Sci. USA*, **97**, 3735–3740.
9. Guo, Y., Halfter, U., Ishitani, M. & Zhu, J. K. (2001). Molecular characterization of functional domains in the protein kinase SOS2 that is required for salt tolerance. *Plant Cell*, **13**, 1383–1399.
10. Quintero, F. J., Ohta, M., Shi, H., Zhu, J. K. & Pardo, J. M. (2002). Reconstitution of the SOS signaling pathway for Na^+ homeostasis in plants. *Proc. Natl Acad. Sci. USA*, **99**, 9061–9066.
11. Qiu, Q., Guo, Y., Dietrich, M. A., Schumaker, K. S. & Zhu, J. K. (2002). Regulation of SOS1, a plasma membrane Na^+/H^+ exchanger in *Arabidopsis thaliana*, by SOS2 and SOS3. *Proc. Natl Acad. Sci. USA*, **99**, 8436–8441.
12. Luan, S., Kudla, J., Rodriguez-Concepcion, M., Yalovsky, S. & Gruissem, W. (2002). Calmodulins and calcineurin B-like proteins, calcium sensors for specific signal response coupling in plants. *Plant Cell*, **14**, S389–S400.
13. Gong, D., Guo, Y., Jagendorf, A. T. & Zhu, J. K. (2002). Biochemical characterization of the *Arabidopsis* protein kinase SOS2 that functions in salt tolerance. *Plant Physiol.* **130**, 256–264.
14. Harmon, A. C., Gribskov, M. & Harper, J. F. (2000). CDPKs—a kinase for every Ca^{2+} signal? *Trends Plant Sci.* **5**, 154–159.
15. Scrase-Field, S. A. & Knight, M. R. (2003). Calcium, just a chemical switch? *Curr. Opin. Plant Biol.* **6**, 500–506.
16. Sutcliffe, M. J., Haneef, I., Carney, D. & Blundell, T. L. (1987). Knowledge based modeling of proteins. 1. 3-Dimensional frameworks derived from the simultaneous superposition of multiple structures. *Protein Eng.* **1**, 377–384.
17. Nagae, M., Nozawa, A., Koizumi, N., Sano, H., Hashimoto, H., Sato, M. & Shimizu, T. (2003). The crystal structure of the novel calcium-binding protein AtCBL2 from *Arabidopsis thaliana*. *J. Biol. Chem.* **278**, 42240–42246.
18. Cyert, M. S. & Thorner, J. (1992). Regulatory subunit (CNB1 gene product) of yeast Ca^{2+}/calmodulin-

dependent phosphoprotein phosphatases is required for adaptation to pheromone. *Mol. Cell. Biol.* **12**, 3460–3469.
19. Schaad, N. C., de Castro, E., Nef, S., Hegi, S., Hinrichsen, R., Martone, M. E. *et al*. (1996). Direct modulation of calmodulin targets by the neuronal calcium sensor NCS1. *Proc. Natl Acad. Sci. USA*, **93**, 9253–9258.
20. Wallace, A. C., Laskowski, R. A. & Thornton, J. M. (1995). LIGPLOT, a program to generate schematic diagrams of protein–ligand interactions. *Protein Eng.* **8**, 127–134.
21. Nooren, I. M. & Thornton, J. M. (2003). Diversity of protein–protein interactions. *EMBO J.* **22**, 3486–3492.
22. Nooren, I. M. & Thornton, J. M. (2003). Structural characterization and functional significance of transient protein–protein interactions. *J. Mol. Biol.* **325**, 991–1018.
23. Lo Conte, L., Chothia, C. & Janin, J. (1999). The atomic structure of protein–protein recognition sites. *J. Mol. Biol.* **285**, 2177–2198.
24. Killian, J. A. & von Heijne, G. (2000). How proteins adapt to a membrane–water interface. *Trends Biochem. Sci.* **25**, 429–434.
25. Monné, M., Nilsson, I., Johansson, M., Elmhed, N. & von Heijne, G. (1998). Positively and negatively charged residues have different effect on the position in the membrane of a model transmembrane helix. *J. Mol. Biol.* **284**, 1177–1183.
26. Lewit-Bentley, A. & Rety, S. (2000). EF-hand calcium-binding proteins. *Curr. Opin. Struct. Biol.* **10**, 637–643.
27. Zhang, M., Tanaka, T. & Ikura, M. (1995). Calcium-induced conformational transition revealed by the solution structure of apo calmodulin. *Nature Struct. Biol.* **2**, 758–767.
28. Kuboniwa, H., Tjandra, N., Grzesiek, S., Ren, H., Klee, C. B. & Bax, A. (1995). Solution structure of calcium-free calmodulin. *Nature Struct. Biol.* **2**, 768–776.
29. Finn, B. E., Evenas, J., Drakenberg, T., Waltho, J. P., Thulin, E. & Forsen, S. (1995). Calcium-induced structural changes and domain autonomy in calmodulin. *Nature Struct. Biol.* **2**, 777–783.
30. Verdino, P., Westritschnig, K., Valenta, R. & Keller, W. (2002). The cross-reactive calcium-binding pollen allergen, Phl p 7, reveals a novel dimer assembly. *EMBO J.* **21**, 5007–5016.
31. Varea, J., Saiz, J. L., Lopez-Zumel, C., Monterroso, B., Medrano, F. J., Arrondo, J. L. *et al*. (2000). Do sequence repeats play an equivalent role in the choline-binding module of pneumococcal LytA amidase? *J. Biol. Chem.* **275**, 26842–26855.
32. Gong, D., Guo, Y., Schumaker, K. S. & Zhu, J. K. (2004). The SOS3 family of calcium sensors and SOS2 family of protein kinases in *Arabidopsis*. *Plant Physiol.* **134**, 919–926.
33. Shi, J., Kim, K. N., Ritz, O., Albrecht, V., Gupta, R., Harter, K. *et al*. (1999). Novel protein kinases associated with calcineurin B-like calcium sensors in *Arabidopsis*. *Plant Cell*, **11**, 2393–2405.
34. Otterbein, L. R., Kordowska, J., Witte-Hoffmann, C., Wang, C. L. & Dominguez, R. (2002). Crystal structures of S100A6 in the Ca(2+)-free and Ca(2+)-bound states, the calcium sensor mechanism of S100 proteins revealed at atomic resolution. *Structure*, **10**, 557–567.
35. Sánchez-Barrena, M. J., Martínez-Ripoll, M., Zhu, J. K. & Albert, A. (2004). SOS3 from *Arabidopsis thaliana*, expression, purification, crystallization and preliminary X-ray analysis. *Acta Crystallog. sect. D*, **60**, 1272–1274.
36. Dunn, M. F., Pattison, S. E., Storm, M. C. & Quiel, E. (1980). Removal of metals from enzyme solutions. *Biochemistry*, **19**, 718.
37. Leslie, A. G. W. (1987). MOSFLM. In *Proceedings of the CCP4 Study Weekend* (Machin, J. R. & Papiz, M. Z., eds), pp. 39–50, SERC Daresbury Laboratory, Warrington, UK.
38. Navaza, J. (1994). AMoRe, an automated package for molecular replacement. *Acta Crystallog. sect. A*, **50**, 157–163.
39. Vagin, A. & Teplyakov, A. (1997). MOLREP, an automated program for molecular replacement. *J. Appl. Crystallog.* **30**, 1022–1025.
40. Bourne, Y., Dannenberg, J., Pollmann, V., Marchot, P. & Pongs, O. (2001). Immunocytochemical localization and crystal structure of human frequenin (neuronal calcium sensor 1). *J. Biol. Chem.* **276**, 11949–11955.
41. Sánchez-Barrena, M. J., Martinez-Ripoll, M., Galvez, A., Valdivia, E., Maqueda, M., Cruz, V. & Albert, A. (2003). Structure of bacteriocin AS-48, from soluble state to membrane bound state. *J. Mol. Biol.* **334**, 541–549.
42. Evans, G. & Bricogne, G. (2003). Triiodine derivatization in protein crystallography. *Acta Crystallog. sect. D*, **59**, 1923–1929.
43. de la Fortelle, E. & Bricogne, G. (1997). Maximum-likelihood heavy-atom parameter refinement for multiple isomorphous replacement and multiwavelength anomalous methods. *Methods Enzymol.* **276**, 472–494.
44. Cowtan, K. & Main, P. (1998). Miscellaneous algorithms for density modification. *Acta Crystallog. sect. D*, **54**, 487–493.
45. Leslie, A. G. W. (1987). A reciprocal-space method for calculating a molecular envelope using the algorithm of B. C. Wang. *Acta Crystallog. sect. A*, **43**, 134–136.
46. Abrahams, J. P. & Leslie, A. G. W. (1996). Methods used in the structure determination of bovine mitochondrial F_1 ATPase. *Acta Crystallog. sect. D*, **52**, 30–42.
47. Brunger, A. T. & Adams, P. D. (1998). Crystallography and NMR system. *Acta Crystallog. sect. D*, **54**, 905–921.
48. Murshudov, G. N., Vagin, A. A. & Dodson, E. J. (1997). Refinement of macromolecular structures by the maximum-likelihood method. *Acta Crystallog. sect. D*, **53**, 240–255.
49. Jones, T. A., Zon, J. Y., Cowan, S. W. & Kjeldgaard, M. (1991). Improved methods for model building in electron density maps and the location of errors in these models. *Acta Crystallog. sect. A*, **47**, 110–119.
50. Bailey, S. (1994). The CCP4 suite, programs for protein crystallography. *Acta Crystallog. sect. D*, **50**, 760–763.
51. Laskowski, R. A., MacArthur, M. W., Moss, D. S. & Thornton, J. M. (1993). PROCHECK, a program to check the stereochemical quality of protein structures. *J. Appl. Crystallog.* **26**, 283–291.
52. Kraylis, P. J. (1991). MOLSCRIPT, a program to produce both detailed and schematic plots of protein structures. *J. Appl. Crystallog.* **24**, 946–950.
53. Merritt, E. A. & Murphy, M. E. P. (1994). Raster3D version 2.0: a program for photorealistic molecular graphics. *Acta Crystallog. sect. D*, **50**, 869–873.
54. Altschul, S. F., Gish, W., Miller, W., Myers, E. W. & Lipman, D. J. (1990). Basic local alignment search tool. *J. Mol. Biol.* **215**, 403–410.

55. Rivas, G., Ingham, K. C. & Minton, A. P. (1994). Ca(2+)-linked association of human complement C1s and C1r. *Biochemistry*, **33**, 2341–2348.
56. Anderson, K. M. & Hovmöller, S. (2000). The protein content in crystals and packing coefficients in different space groups. *Acta Crystallog. sect. D*, **56**, 789–790.
57. Sayle, R. A. & Milner-White, E. J. (1995). RasMol, biomolecular graphics for all. *Trends Biochem. Sci.* **20**, 374–376.

Edited by R. Huber

(Received 17 September 2004; received in revised form 5 November 2004; accepted 10 November 2004)